J Mol Model (2014) 20:2537
DOI 10.1007/s00894-014-2537-5

ORIGINAL PAPER

Structure, vibrational, and optical properties of platinum cluster: a density functional theory approach

Ngangbam Bedamani Singh · Utpal Sarkar

Received: 7 March 2014 / Accepted: 17 November 2014 / Published online: 2 December 2014

Abstract Using density functional theory, stability, chemical, and optical properties of small platinum clusters, Pt_n (n=2 to 10) have been investigated. An attempt has been made to establish a correlation between stability and chemical reactivity parameters. The calculated geometries are in agreement with the available experimental and theoretical results. The atom addition energy change (ΔE_1) and stability function (ΔE_2) reveal that Pt_7 is more stable than its neighboring clusters. Very good agreement of the calculated electron affinity with the available experimental results has been observed. The polarizability of the Pt_n clusters depends almost linearly on the number of atoms. A correlation between the static polarizability and ionization potential is found, paving a way to calculate polarizabilty of larger clusters from their ionization potential. The calculated vibrational frequencies are compared with available experimental and theoretical results and good agreement between them has been established. In general, the prominent peak of molar absorption coefficient is shifting toward the lower energy side when cluster size grows. Our DOS calculation suggests that *d* orbital is primarily responsible for HOMO position and *s* orbital is responsible for LUMO position.

Keywords Chemical reactivity · Density functional theory · Metal clusters · Optical property · Stability

Electronic supplementary material The online version of this article (doi:10.1007/s00894-014-2537-5) contains supplementary material, which is available to authorized users.

N. B. Singh · U. Sarkar (✉)
Department of Physics, Assam University, Silchar 788011, India
e-mail: utpalchemiitkgp@yahoo.com

Introduction

The study of small metal cluster is of major interest to both theoreticians and experimentalist, because it provides a link between the molecular state and the solid state. Compared to their bulk counterparts, metal clusters are known to possess enhanced reactivity, which make them attractive for catalysis. Small transition metal clusters have a wide range of applications and serve as building blocks of functional nanostructured materials, electronic devices, nanocatalysts, and other fields of nanotechnology [1, 2]. Their unique catalytic activities are attributed to the large fraction of low-coordinated surface atoms [3].

Transition metal clusters like Pt, Rh, and Pd are used to reduce toxic pollutants, such as CO, NO, and hydrocarbons in automotive exhaust systems [4]. Platinum along with Ni and Pd, are used as catalysts in many industrial processes. Since Pt clusters have small hydrogenation energy compared with other metal clusters, they are used in many catalytic reactions such as hydrogenation, dehydrogenation, and cracking of various hydrocarbons [5]. It is the preferred oxidation and reduction catalyst for low-temperature proton exchange membrane (PEM) fuel cells [6]. It is also an excellent catalyst for a number of electrochemical reactions related to fuel cells, e.g., for oxidation of formic acid [7], methanol [8], and also for the reduction of oxygen [9].

The shape and the microstructure play a major role in controlling the catalyst's activity. With the decrease of the size, the catalytic activities of Pt tend to increase because of the increased surface area of smaller particle and the structural sensitivity of some reactions [10]. The reactivity of clusters is sensitive to size and shape [11, 12]. The study of the mechanical, chemical, and electromagnetic properties of the platinum clusters and their relationships to size and shape will enhance our understanding of these small clusters and also their applications in the chemical and material industry. These small

clusters can serve as the model and help in understanding the property evolution as they grow from small nanoscale size to bulk. As the experimental determination of structure and specific electronic characterizations of these nanoscale systems are quite difficult; one has to rely on the predictive power of computational methods. Accurate theoretical prediction of the cluster structures is therefore essential. In addition, accurate prediction of vibrational frequency, IR intensity, and Raman activity facilitates in identifying the true cluster geometries, since the agreement between theoretical and experimental spectra confirms that the theoretically predicted structures are true.

In the case of platinum clusters, structure prediction becomes quite challenging because of competition between spin exchange stabilization and electron correlation effects [13]. These two effects tend to alter the electronic states and the structural properties as a function of theoretical treatment. Moreover, the open *d* shell of these clusters generates several electronic states with varied spin multiplicities and geometries which make the investigation of structural and spectroscopic properties of these clusters difficult [14]. The cluster size [15] and sometimes their symmetries [16] could be inferred from experiments, but the microscopic descriptions of their structure are far from definitive.

Despite many experimental and theoretical works about structure, chemical, and magnetic properties, the study of the optical response of small Pt clusters has not been performed to our knowledge. The investigation of optical response may provide much useful information about the dynamic properties of Pt clusters. The spectra are calculated using ab initio TDDFT on the ground state geometries of Pt clusters up to ten atoms. The purpose of this study is to understand the structure, stability, and reactivity of small platinum clusters (Pt_n, n=2 to 10) and is to shed some light on the unique nature and properties of these small transition metal clusters.

Theoretical background

Based on density functional theory (DFT), the stability, aromaticity, and chemical reactivity of atoms, molecules, and clusters can be successfully explained [17–31]. Within DFT framework the ionization potential (*IP*) and electron affinity (*EA*) can be calculated using the finite difference approach as [17]:

$$IP = E(N-1) - E(N) \tag{1}$$

and

$$EA = E(N) - E(N+1) \tag{2}$$

where *E(N-1)*, *E(N)*, and *E(N-1)* are the energies of the (N-1), N, and (*N*+1) electron systems.

Chemical potential (μ) [17] and chemical hardness (η) [18] are determined in terms of *IP* and *EA* as:

$$\mu = -\frac{IP + EA}{2} \tag{3}$$

$$\eta = \frac{IP - EA}{2} \tag{4}$$

Electrophilicity index (ω), which, *measures the stabilization in energy when the system acquires an additional electronic charge from the environment,* is defined as [19–21]:

$$\omega = \frac{\mu^2}{2\eta} \tag{5}$$

The static electric dipole polarizability (α) is the second-order variation of energy (E) with respect to the applied electric field (F) and is defined as:

$$\alpha_{a,b} = -\left(\frac{\partial^2 E}{\partial F_a \partial F_b}\right); a, b = x, y, z \tag{6}$$

and the static dipole polarizability is computed as the trace of the polarizability tensor as follows:

$$< \alpha > = \frac{1}{3}\left(\alpha_{xx} + \alpha_{yy} + \alpha_{zz}\right) \tag{7}$$

These parameters can be properly understood in terms of their related electronic structure principles like the minimum polarizability principle (MPP) [22, 23] and the minimum electrophilicity principle (MEP) [24–26], etc.

In order to analyze stability and energetic of the cluster, the binding energy per atom (E_b) is calculated as:

$$E_b = E_{atom} - \frac{E_{cluster}}{n} \tag{8}$$

where n is the number of atoms in the cluster and E_{atom} and $E_{cluster}$ are the energies corresponding to single atom and cluster respectively. The atom addition energy change which corresponds to the energy change in cluster growing reaction is described as:

$$\triangle E_1(Pt_n) = E(Pt_n) - E(Pt_{n-1}) - E(Pt) \tag{9}$$

A large negative change implies that the cluster Pt_n is more stable than the preceding Pt_{n-1} structure. To analyze the relative stability, the second finite difference of total energies (i.e., the stability function) is computed as:

$$\triangle E_2(Pt_n) = E(Pt_{n+1}) + E(Pt_{n-1}) - 2E(Pt_n) \tag{10}$$

The photoabsorption cross section has been calculated using the relation [32]:

$$\sigma(E) = \frac{\pi e^2}{2mc\varepsilon_o}\sum_{i\neq 1}^{N_{fs}}\left[\frac{1}{N_p^l}\sum_k^{N_p^l} f_{il}(R_k)g(E-\Delta E_{il}(R_k),\delta)\right] \quad (11)$$

where m is the mass of an electron, e is its charge, c is the velocity of light, $\mathcal{E}_o$ is the vacuum permittivity, and $E=\hbar\omega$ is the radiation energy for an angular frequency ω. The transition energy ΔE_{il} and oscillator strengths f_{il} corresponding to transitions from initial state i to final state l are computed for each point in the $\{R_k\}$ ensemble. We have convoluted the intensity with a normalized line shape function $g(E\text{-}\Delta E_{il}(R_k),\delta)$ peaked at the transition energy.

Computational method

Initial geometries for each of the cluster size of platinum clusters Pt_n (n=2–10) are generated using a constant temperature ab-initio molecular dynamics run using SIESTA 3.1 [33] near the melting temperature of bulk platinum. Ab-initio molecular dynamics are carried out in the NVT ensemble and temperature is controlled using Nose thermostate. Newton's equations of motion are integrated using the Verlet algorithm with a time step of 1.00 fs. The molecular dynamics simulatons were carried out for 5000 fs at a temperature of 2000 K (melting point for Pt≈2046 K). During the simulation process, the structure of the cluster goes through various changes. Based on low energy criteria, we chose some of these structures with reasonably different geometry. We have also considered those ground state geometries reported in the literature for Pt cluster. The calculations are performed in the framework of density functional theory employing the GAUSSIAN 09 suite of program [34]. In this study, we have used B3LYP [35, 36] and B3PW91 [35, 37] functionals. The relativistic Los Alamos National Laboratory effective core potentials as well as DZ atomic basis set (LanL2DZ) [38], which uses relativistic effective core potentials (ECP) to reduce the number of electrons are used in the calculation. In order to see the effects of basis set on the calculated properties, we also used LanL2MB [38–40] basis set.

We have first performed optimization of the neutral clusters. It was followed by single point calculations of the positively and negatively charged clusters having the same optimized geometry as the neutral clusters to determine the vertical ionization potentials and electron affinities. The TDDFT calculations are performed on the ground state geometries of DFT calculations. The calculation of photoabsorption cross section has been carried out using the methods implemented in NEWTON-X program [41, 42].

Results and discussion

To test the reliability of our method, we first calculated the *IP* for the single platinum atom. The experimental value for the single Pt atom is reported as 8.80±0.2 eV [43] and our calculated *IP* with B3LYP functional and LanL2DZ basis set is 8.75 eV. Other calculation levels give *IP* values as 8.51 eV (B3LYP/LanL2MB), 8.70 eV (B3PW91/LanL2DZ), and 8.44 eV (B3PW91/LanL2MB). As we can see, *IP* value given by B3LYP/LanL2DZ is closest to the experimental value, we will discuss the properties calculated using B3LYP/LanL2DZ method and the other methods are reported to make comparisons with B3LYP/LanL2DZ results. The most stable structures of platinum clusters up to ten atoms are shown in Fig. 1. A number of low lying isomers with closely separated energies are observed for each given size of the platinum clusters and are presented in Fig. S1 in the supplentary material .

We have seen that Pt_2 have a triplet ground state with a bond length of 2.37 Å the same as obtained by Fortunelli [44] by DFT calculation. It is found in the $D_{\alpha h}$ symmetry and has a binding energy per atom, E_b=1.40 eV/atom. Experimentally, Grushov and Ervin [45] have reported the bond length of Pt_2 as 2.33 Å and E_b=1.57 eV/atom. Pt_3 has the lowest energy structure of an equilateral triangle (Fig. 1) with bond length 2.52 Å, E_b=1.85 eV/atom, and triplet spin multiplicity. An isosceles triangle (S1 ii [a]) and linear shaped (S1 ii [b]) are 0.10 and 2.10 eV higher in energy than the equilateral triangle. Yang et al. [46] have found an equilateral triangle with bond length 2.58 Å as the ground state of Pt_3 having E_b=2.40 eV/atom. Kumar and Kawazoe [47] have also found an equilateral triangle with bond length 2.49 Å as the ground state of Pt_3. For Pt_4, the structure having minimum energy is a bent rhombus (Fig. 1) with bond length 2.51 Å and singlet spin multiplicity with E_b=2.11 eV/atom. Kumar and Kawazoe [47] have also reported a bent rhombus with bond length 2.51 Å as the lowest energy structure for Pt_4. A tetrahedron (S1 iii [a]) is 0.31 eV higher in energy and a square (S1 iii [b]) lies 0.36 eV higher than bent rhombus. The lowest energy structure of Pt_5 is a planar side-capped square (Fig. 1) which has triplet spin and binding energy E_b=2.14 eV/atom. Kumar and Kawazoe [47] have also reported side-capped square as the most favored geometry for Pt_5. A square pyramid (S1 iv [a]) lies 0.06 eV higher in energy and a trigonal bipyramid (S1 iv [b]) is 0.11 eV higher in energy. We have found the most stable structure of Pt_6 as planar triangular shaped structure (Fig. 1), the same as other DFT calculations [46, 47] and having pentet spin multiplicity with E_b=2.23 eV/atom. A double square (S1 v [a]), prism shaped (S1 v [b]), and octahedron are 0.29, 0.39, and 0.45 eV higher in energy than the most stable structure. The lowest energy structure of Pt_7 is of the shape of two fused square pyramids (Fig. 1) and has quintet state with E_b= 2.41 eV/atom. Tian et al. [48] have also obtained similar ground state structure for Pt_7. A prism capped on triangular

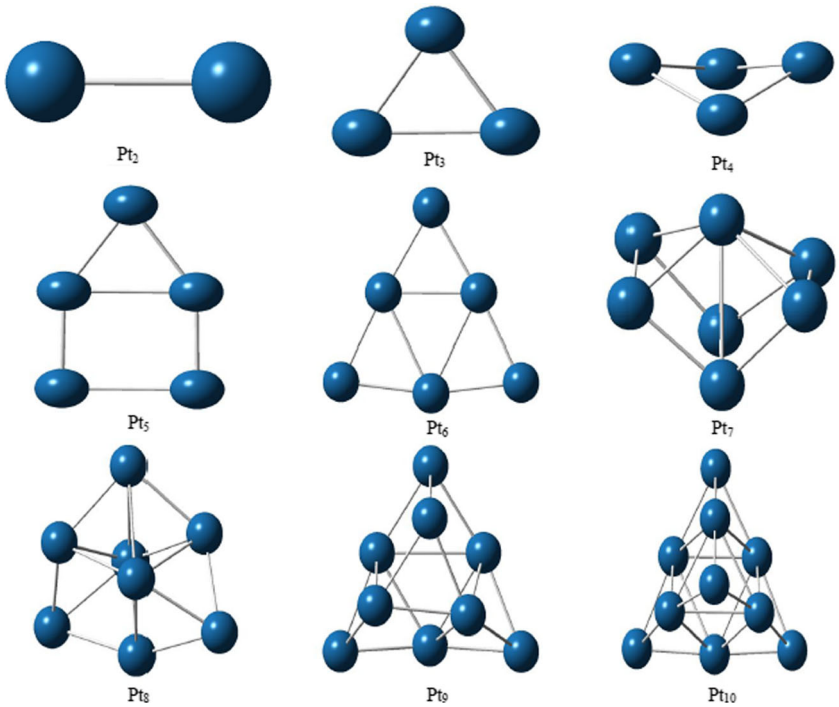

Fig. 1 Most stable structures of Pt_n (n=2 to 10) clusters

face (S1 vi [a]) lies only 0.13 eV higher in energy, while a prism capped at center of the edge is 0.18 eV higher. A planar side capped double square (S1 vi [b]) which was observed as the most stable structure by Kumar and Kawazoe [47] lies 0.92 eV higher in energy than the most stable structure of Fig. 1. The lowest energy structure of Pt_8 is a hexagonal bipyramid (Fig. 1) and has septet spin with E_b=2.47 eV/atom. Kumar and Kawazoe [47] have also reported hexagonal bipyramid as the lowest energy structure for Pt_8. A cubic structure (S1 vii [a]), a bicapped octahedron and a double square bicapped on the long edge (S1 vii [b]) are 0.64, 0.80, and 1.23 eV higher in energy than the hexagonal bipyramid. The most stable structure of Pt_9 is tricapped octahedron (Fig. 1), having nonet spin and E_b=2.59 eV/atom. An isomer formed of fused square pyramids (S1 viii [a]) lies 0.90 eV higher in energy. A planar isomer with four squares (S1 viii [b]) which Kumar and Kawazoe [47] observed as the minimum energy structure for Pt_9 lies 2.04 eV higher than the tricapped octahedron. The lowest energy structure of Pt_{10} is a tetracapped octahedron (Fig. 1) in agreement with the geometries of Kumar and Kawazoe [47] having nonet spin multiplicity and E_b=2.71 eV/atom. An isomer which can be considered as a distorted tetrahedron formed from fused square pyramid and prism (S1 ix [a]) lies 0.63 eV higher in energy and a bicapped cube isomer (S1 ix [b]) lies 0.74 eV higher. Hence planar isomers are obviously not favored for Pt_n clusters with n>6. The binding energy of the cluster increases with cluster size.

Atom addition energy change (ΔE_1) and stability function (ΔE_2) are plotted as a function of cluster size in Fig. 2a. It is seen that Pt_7 have high ΔE_2 value and large negative value of ΔE_1 indicating it is more stable than their neighboring clusters. The electron affinity (*EA*) and electrophilicity (ω) values for Pt_n clusters as a function of cluster size are shown in Fig. 2b. The experimental value of *EA* reported for Pt atom is 2.12 eV [49], which is in reasonable agreement with our B3LYP/LanL2DZ calculated value of 2.21 eV. The *EA* for Pt_2 is calculated to be 1.94 eV which is very close to the experimental result of 1.898±0.008 eV, reported by Ho et al. [50]. *EA* for the Pt_3 is 2.09 eV, which is consistent with the experimental observation 1.89 eV by Ervin et al. [51] and 1.8± 0.1 eV by Pontius [52]. Our calculated *EA* value 2.22 eV, for Pt_4 is in agreement with the experimentally reported value 2.5±0.1 eV [52]. *EA* for Pt_5 is calculated as 2.54 eV which agrees well with the experimental value of 2.63± 0.1 eV [52]. *EA* values for Pt_6, Pt_7, Pt_8, Pt_9, and Pt_{10} are calculated as 3.53, 2.94, 2.93, 1.95, and 1.91 eV respectively. Since *EA* is a measure of the tendency of a system to attract electrons, stable systems are least expected to acquire electrons and hence have low *EA* values. Thus, the abrupt decrease in *EA* when going from Pt_6 to Pt_7 is because of higher stability of Pt_7 cluster as also seen from the values of ΔE_1 and ΔE_2. The ionization potential (*IP*) values are tabulated in Table 1, the *IP* values for Pt_n (n=2–10) are in the range between 9.31 and 7.36 eV. Overall, the IP values are seen to decrease with increasing cluster size. A study based on image-charge model also reorted that the electron removal energy decreases with increasing cluster size [53]. It may be mentioned here that experimentally determined *IP* for Pt atom is 8.80±0.2 eV [45] and work function for bulk Pt metal is 6.10±0.6 eV [54].

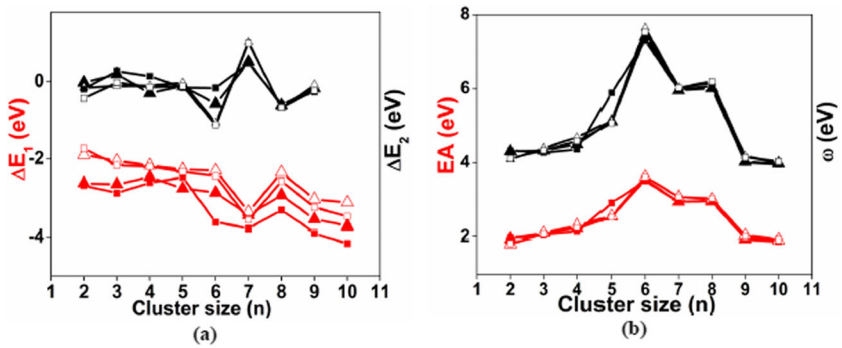

Fig. 2 **a** Variation of atom addition energy change (ΔE_1) and stability function (ΔE_2) with cluster size. Red color represents atom addition energy change (ΔE_1) and black color represents stability function (ΔE_2). Irrespective of color, solid triangle (▲) represents B3LYP/LanL2DZ, solid rectangle (■) represents B3PW91/LanL2DZ, hollow triangle (△) represent B3LYP/LanL2MB a,nd hollow rectangle (□) represent B3PW91/LanL2MB. **b** Variation of electron affinity (*EA*) and electrophilicity (ω) with cluster size. Red and black color represent electron affinity (*EA*) and electrophilicity (ω) respectively. See the caption of Fig. 2a for details

The electrophilicity is a measure of the stabilization in energy when the cluster acquires an additional electronic charge from the surroundings. It is evident from Fig. 2b that ω is closely related to *EA* and shows similar variation in changing cluster size. Stable systems, i.e., less reactive systems are expected to have low electrophilicity values because they are less likely to acquire additional electronic charge so as to become more stable. The ω value of Pt_7 is lower than its neighboring clusters, which supports its relative higher stability as seen from (ΔE_1) and (ΔE_2). The observed electrophilicity value of Pt_7 clusters is in agreement with the minimum electrophilicity principle (MEP) [24–26] which states that "electrophilicity will be a minimum (maximum) when both chemical potential and hardness are maxima (minima)".

Polarizability can provide information about the electronic properties and structural geometry of the clusters as they are very sensitive to the delocalization of valence electrons and structural geometry. The theoretical prediction of polarizabilities and comparison with the experimental values, enable one to identify which cluster is being observed in the experiment. The polarizabity for single Pt atom is 44 a. u. (atomic units)

Table 1 Ionization potential (***IP***), HOMO-LUMO gap (E_g), and binding energy per atom (E_b) of Pt_n (n=2 to 10) clusters calculated using B3LYP/LanL2DZ method

Cluster	***IP*** (eV)	E_g (eV)	E_b (eV/atom)
Pt_2	9.31	3.01	1.40
Pt_3	8.12	1.85	1.85
Pt_4	7.84	1.96	2.02
Pt_5	8.25	2.07	2.14
Pt_6	8.07	1.49	2.23
Pt_7	7.62	1.22	2.41
Pt_8	7.36	1.37	2.47
Pt_9	7.51	2.79	2.59
Pt_{10}	7.56	2.92	2.71

[55], which is very close to our calculated result of 41.51 a.u. The calculated static polarizabilities per atom of the platinum clusters are presented in Fig. 3a. The polarizability of the Pt_n clusters depends almost linearly with regression coefficient of 0.996 (B3LYP/LanL2DZ), 0.997 (B3LYP/LanL2MB), 0.996 (B3PW91/LanL2DZ), and 0.997 (B3PW91/LanL2MB) on the cluster size. Mohajeri et al. [56] have shown that ZnS clusters which have lower polarizability per atom with respect to the neighboring clusters are relatively more stable than the neighboring clusters. The observation of minimum at n=7 is consistent with previous results of stability function and electrophilicity and also in accordance with the minimum polarizability principle [22, 23]. To check the correlation between the static polarizability and ionization potential, we have plotted cube root of the polarizability as a function of the inverse of ionization potential in Fig. 3b. It is evident form Fig. 3b that the cube root of the polarizability increases linearly with increasing inverse of the ionization potential with a linear correlation coefficient of 0.989 (B3LYP/LanL2DZ), 0.998 (B3LYP/LanL2MB), 0.989 (B3PW91/LanL2DZ), and 0.997 (B3PW91/LanL2MB), thereby indicating the reliability of the correlation. It is an interesting finding, paving a way to calculate polarizabilty of larger clusters from their ionization potential.

The vibrational frequency of Pt_2 in our calculation has been found as ω_c=225.59 cm^{-1} and it corresponds to the stretching mode between the two platinum atoms. Jansson and Scullman [57] measured vibrational spectrum in Ar matrix, and observed single vibronic transition at ω_c=217.20 cm^{-1}. Using ab initio calculation, Yang et al. [46] have computed the vibrational frequency of Pt_2 as ω_c=218.00 cm^{-1}. We found the vibrational modes of the ground state of Pt_3 at 140.76 and 187.36 cm^{-1}. The first mode appearing at 140.76 cm^{-1} is due to the stretching mode of two Pt-Pt bonds, while the third bond remains fixed. Another vibrational mode at 187.36 cm^{-1} corresponds to the stretching mode of the three bonds in the ground state of Pt_3 cluster. Photoelectron spectroscopic study

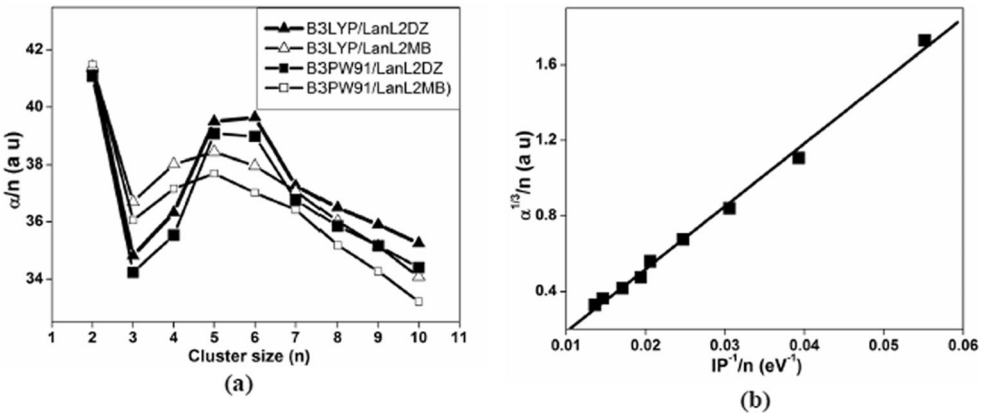

Fig. 3 **a** Static polarizability per atom as a function of cluster size. **b** Correlation between cube root of polarizabity and inverse of ionization potential for platinum clusters

of Pt_3 by Ervin et al. [51] confirmed peaks at frequencies 105±30 and 225±30 cm^{-1}while ab initio study by Yang et al. [46] obtained the vibrational modes at 145.00, 215.00, and 290.00 cm^{-1}. For Pt_4, the peaks of vibrational frequency are observed at 27.66, 46.21, 172.71, 172.73, and 190.88 cm^{-1}. The lowest vibrational frequencies for Pt_5, Pt_6, Pt_7, Pt_8, Pt_9, and Pt_{10} are observed at 18.76, 18.78, 11.43, 17.63, 26.08, and 33.48 cm^{-1} respectively, and the highest vibrational frequencies are found at 188.26, 226.92, 176.35, 179.25, 199.94, and 202.68 cm^{-1} respectively.

Since Raman spectroscopy is very sensitive to the structure, we have used it in this study and is presented in Fig. 4. There is only one peak in Pt_2 which is observed at 234.00 cm^{-1} (Fig. 4a). This Raman peak corresponds to the stretching mode between the two platinum atoms of Pt_2. The Raman spectra for the Pt_3 (Fig. 4b) have two distinct peaks at 147.00 and 228.00 cm^{-1}. The first peak appearing at 147.00 cm^{-1} is due to the stretching mode of two Pt-Pt bonds, while the third bond remains fixed. The highest peak at 228.00 cm^{-1} corresponds to the stretching mode of the three bonds in the ground state of Pt_3 cluster. The Pt_4 has four dominant peaks emerging in between 28.00 and 198.00 cm^{-1} (Fig. 4c). The highest peak is observed at 198.00 cm^{-1} and is assigned to the symmetric stretching mode of the Pt atoms. The other distinct peak appearing at 177.00 cm^{-1} is assigned to the antisymmetric stretching mode. For Pt_5, the observed Raman spectra shows a number of peaks in between 90.00 and 240.00 cm^{-1}, with highest peak at 236.00 cm^{-1} (see Fig. S2 of the supplementary material). In the case of Pt_6, the maximum peak at 158.00 cm^{1} is assigned to the symmetric stretching of all the bonds (shown in Fig. S2 of the supplementary material). The Raman spectra for Pt_7, Pt_8, Pt_9, and Pt_{10} show maximum peaks at 177.00, 184.83, 166.00, and 159.96 cm^{-1} respectively (see Fig. S2 of the supplementary material).

Optical spectroscopy is one the most powerful instrument to investigate the electronic and thermodynamic properties. Theoretical investigations of optical properties are usually done by employing TDDFT methods, in which all or at least the valence electrons are treated accurately. We have calculated the spectra for cluster geometries having lowest energy. Each cluster is observed to show their characteristic optical absorption bands as the geometry of the clusters are drastically different from one another. In Fig. 5, the oscillator strengths (*f*) and molar absorption coefficient ( ) of the cluster ground state of Pt_2 and Pt_3 are presented. The absorption spectrum of Pt_2 (Fig. 5a) shows maxima at λ=512.82 nm which lies in the visible region and for Pt_3, the maximum peak is observed at λ=528.63 nm of the

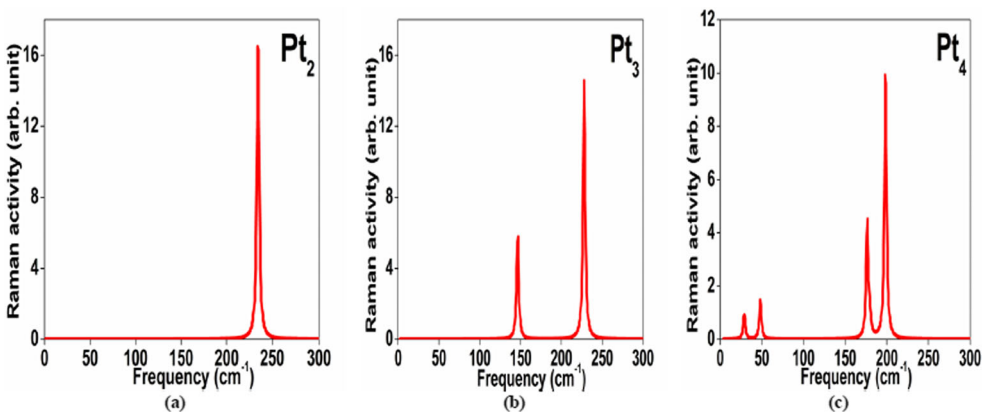

Fig. 4 Raman spectra of platinum clusters

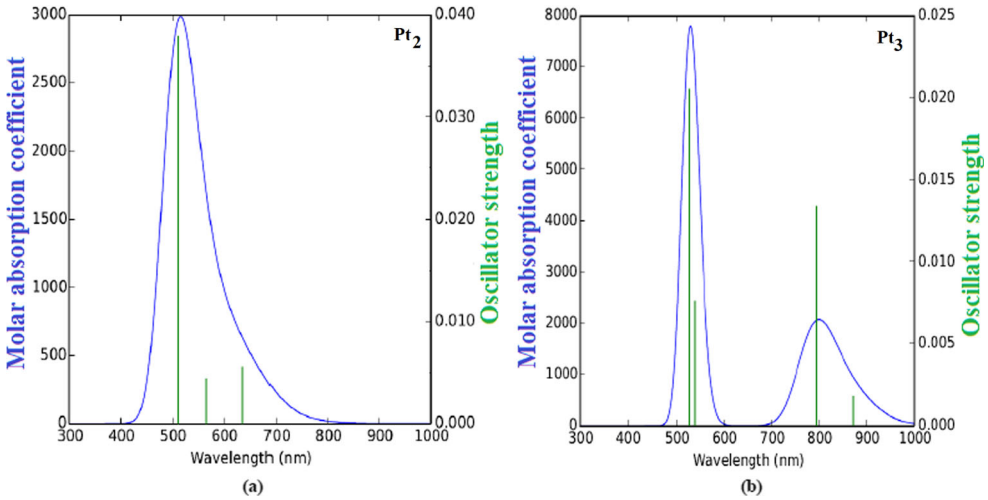

Fig. 5 Oscillator strengths (atomic unit) and molar absorption coefficient ($mol^{-1}dm^3cm^{-1}$) of the most stable platinum clusters

visible region (Fig. 5b) followed by another significant peak at 794.92 *nm*. The absorption spectra for Pt_4 shows two significant peaks: one at 6.33.25 nm and another at 998.86 nm. The former one having the highest peak with oscillator strength 0.0159 and the latter one with diminished peak with oscillator strength 0.0091. For larger clusters with $n>4$, the peaks are observed in the infra red region (shown in Fig. S3 of the supplementary material). The overall evolutionary trend of the most prominent peak occurs at higher wavelength (or low energy) side once we move toward larger cluster size and also the onset of absorption shifted toward the low energy side with increasing the size of the cluster.

The photoabsorption spectra of clusters are mainly determined by the collective plasmon excitation of delocalized electrons and the resonant transition of electrons bounded to the atom. In this study, we report transition up to the first five excited states which includes both single photon and multi-photon transitions. In Pt_2, the single photon transitions are observed for the excited states, one and two, with same transition energy 0.156 eV and oscillator strength 0.0003 eV. Single photon transition is also observed for excited state 4 with energy 0.1907 eV and oscillator strength 0.0003 eV. Multi photon transitions are observed for excited states 3 and 5 with transition energies 0.1907 and 0.5855 eV respectively.

Pt_3 shows two single-photon excitations with energy 0.4569 eV (oscillator strength 0.0003 eV) at excited states 2 and 3. Excited states 1 (energy 0.345 eV), 4 (energy 0.483 eV), and 5 (energy 0.483 eV) are multi-photon excitations. In the cases of Pt_4, Pt_5, and Pt_6, only one single-photon transition has been observed at excited state 4 with oscillator strength 0.0018, 0.0003, 0.0003 eV and energy 0.6683, 0.448, 0.5468 eV respectively. Others are multi-photon transitions. The transitions for excited states 1, 2, 3, and 5 of Pt_5 are with energies 0.312, 0.353, 0.379, and 0.465 eV respectively, and that of Pt_6 are 0.263, 0.444, 0.469, and 0.560 eV respectively.

Single-photon excitations are observed for excited states 1, 4, and 5 with energies 0.341, 0.648, and 0.679 respectively and multi-photon transitions are observed for excited states 2 and 3 with energies 0.452 and 0.508 eV respectively for Pt_7 cluster. Pt_8 has one single-photon transition at excited state 4 with energy 0.465 eV. The multi-photon transitions for Pt_8 have been observed at energies 0.311, 0.418, 0.422, and 0.466 eV for excited states 1, 2, 3, and 5 respectively. In the case of Pt_9, all the excitations up to excited state 5 are multi-photon excitations with energies 0.524, 0.543, 0.568, 0.590, and 0.635 eV respectively. First single-photon excitation is seen at excited state 7 with energy 0.719 eV. Pt_{10} has single-photon transitions at excited state 7 with energy 0.878 eV, all the excitations up to excited state 5 are multi-photon excitations with energies 0.467, 0.489, 0.517, 0.535, and 0.572 eV respectively. The sum of the oscillator strengths characterizes the valence electron delocalization rate. The sum of the oscillator strength which characterizes the valence electron delocalization rate, for the clusters are obtained as 0.157 (Pt_2), 0.221 (Pt_3), 0.189 (Pt_4), 0.009 (Pt_5), 0.009 (Pt_6), 0.012 (Pt_7), 0.004 (Pt_8), 0.007 (Pt_9), 0.002 (Pt_{10}) eV. It may be noted here that the valence electron delocalization rate for the smaller clusters (Pt_2, Pt_3, and Pt_4) are higher than those of larger clusters.

The photoabsorption cross sections are presented in Fig. 6 and Fig. S4 of the supplementary material. The peaks of the photoabsorption curves are observed in the region 0.15 to 0.80 eV and may be due to the resonant excitation of the plasma oscillations of the cluster electrons [58]. From Fig. 6a, b, and c, we can see that the photoabsorption spectra of Pt_2 show strong resonances near 0.15 eV, Pt_3 near 0.47 eV and Pt_4 near 0.82 eV. Apart from the main photoabsorption peak, Pt_3 shows additional secondary peaks in the energy range 1.05 to 1.40 eV, and Pt_4 shows additional secondary peak near 0.67 eV. For Pt_5 and Pt_8, the absorption curve shows strong resonances in the vicinity of 0.47 eV (Fig. S4 of the supplementary material). The

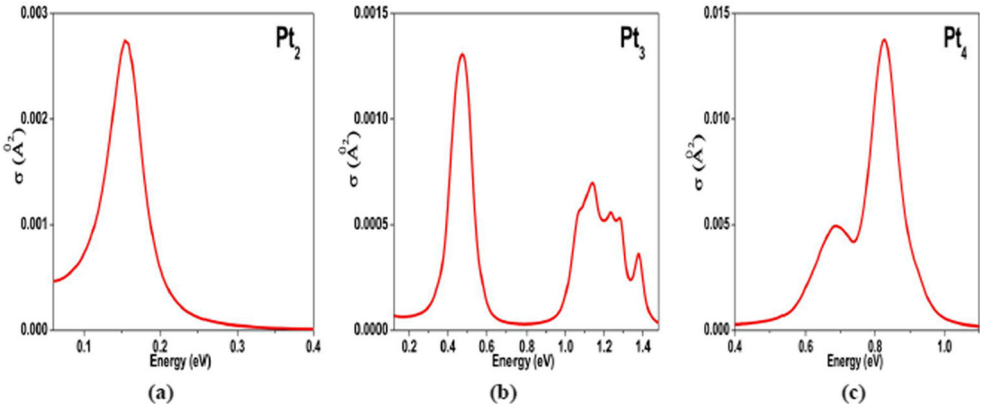

Fig. 6 Photoabsorption cross section calculated for the most stable platinum clusters

absorption curves of Pt_6, Pt_7, and Pt_9 show strong resonances around 0.70 eV. In the case of Pt_{10}, the photoabsorption curve shows a strong peak at 0.66 eV, another very prominent peak is also observed at 0.44 eV.

The transition metal clusters are especially useful in catalysis because of their incomplete *d* shell electronic structure. Their reactivity depends on the arrangement of electrons and there exists a size induced metal–insulator transition in metal clusters. When the size of the metal cluster reduces, the energy level spacing becomes prominent resulting in a large HOMO-LUMO gap. The density of states gives the detailed electronic structure of the clusters and therefore, can shed light on the reactivity of the clusters. Only the energy states close to the HOMO and LUMO have an appreciable influence on the chemical reactivity of the cluster. Here we discuss DOS for the ground states of Pt_n (n=2, 3, and 4) to get a general overview (DOS for Pt_n; n>4 are presented in Fig. S5 of the supplementary material).

The discreteness of the DOS for Pt_n cluster is observed here. Figure 7a shows the density of states of Pt_2 cluster, where high intense peaks are distributed around −8.00 to −7.00 eV. For Pt_2, the HOMO energy is at -6.90 eV and LUMO energy is at −3.89 eV. The main contribution of HOMO is coming from *s* and *d* orbitals; *d* orbital's contribution is highest and *s* orbital is also reasonably contributed. In the case of LUMO, opposite trend has been found; here *s* orbital's contribution is higher than *d* orbital's contribution. In Fig. 7b, the total and projected density of states for Pt_3 is shown. The high intensity peaks in the energy range −7.60 to –5.70 eV are mainly contributed by *d* orbital with a small contribution from *s* and *p*. The HOMO energy is at -5.88 eV and LUMO energy is at -4.03 eV. In the HOMO region, the contribution from *d* orbital is highest, with very small contributions from *s* and *p* orbitals. However, in the LUMO region, the dominant orbital which contributes most is the *p* orbital and contribution from *s* and *d* orbitals are almost negligible. For Pt_4, the calculated DOS is presented in Fig. 7c where HOMO and LUMO energies are at −5.88 and −3.92 eV respectively. A similar trend (as in Pt_3) is seen for the HOMO region of Pt_4 with *d* orbital's contribution being highest in this region where as *s* and *p* orbital's contribution comparatively very less. In the LUMO region, contribution comes from all the *s*, *p*, and *d* orbitals and the contribution is in the order $d > s > p$.

In order to understand the nature of bonding in the cluster, the crystal orbital overlap population (COOP) [59] analysis has been carried out. COOP can be used to quantify the bonding between two orbitals where positive and negative value signifies bonding and antibonding interactions. The COOP for Pt_2 given in Fig. 8a shows that in the energy range

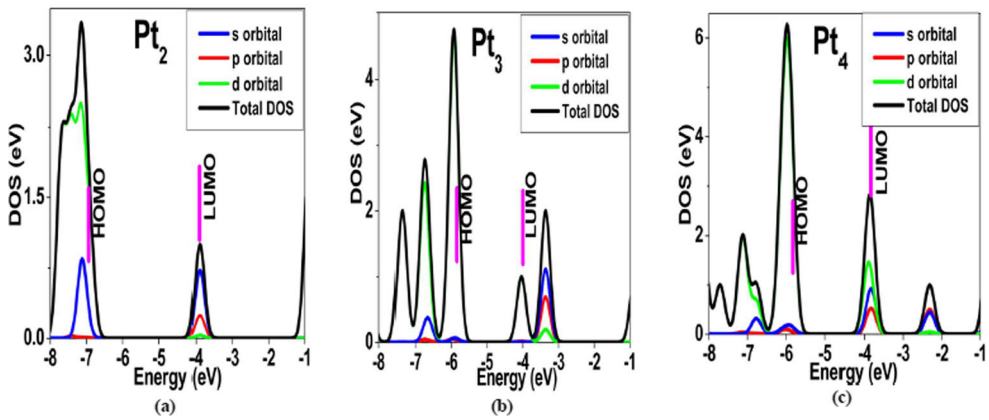

Fig. 7 Total and projected density of states for the most stable platinum clusters

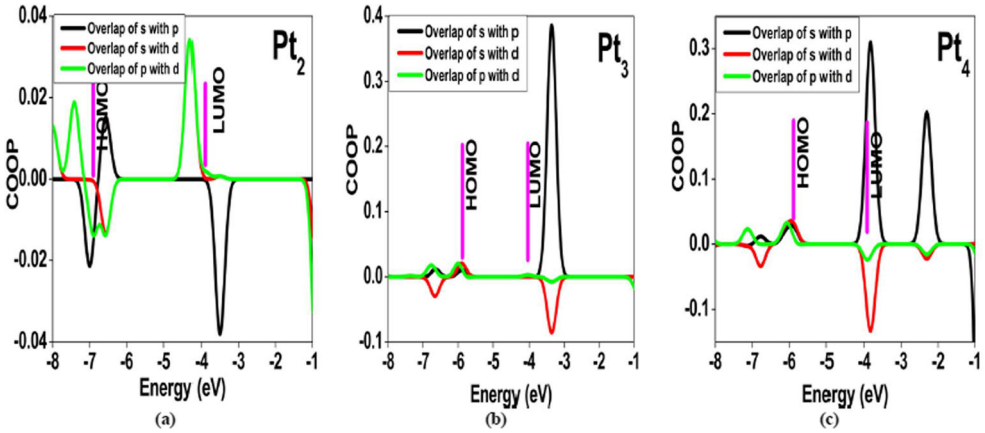

Fig. 8 Crystal orbital overlap population (COOP) of the most stable platinum cluster

−7.70 to −7.20 eV, there is strong bonding interaction with large overlap between *p* and *d* orbitals. Interaction of *s* with *p* orbital and *p* with *d* orbital results to antibonding states in the energy range from −7.15 to −6.80 eV including the HOMO (−6.90 eV) level. As we move a little more above the HOMO, the energy states from −6.75 to −6.25 eV have bonding interaction due to *s* and *p* orbital overlapping. Antibonding interactions are originated from the overlap of *s* with *d* orbital and *p* with *d* orbital in this energy range (i.e., −6.75 to −6.25 eV). Bonding interactions are observed between *s* with *d* orbital and *p* with *d* orbital at the lower energy side of LUMO (in the energy range −4.00 to −4.55 eV). At the LUMO (−3.89 eV) level, very weak bonding interaction is seen between *p* and *d* orbitals. On the other hand, if we move toward higher energy side from LUMO (in the energy region −3.80 to −3.20 eV), antibonding interaction is observed between *s* and *p* orbitals.

In Fig. 8b, the COOP diagram for Pt_3 cluster is presented. Here, it is seen that weak bonding interactions, because of overlapping of *s* with *p* and *p* with *d*, are formed in the energy region −6.90 to −6.50 eV, i.e., on the lower energy side of HOMO. In the same region, antibonding states are also seen due to *s* and *d* orbital interaction. At the HOMO (−5.88 eV) region, weak bonding interactions are formed due to overlapping of *s* with *p* orbital, *s* with *d* orbital, and *p* with *d* orbital. In contrary, no bonding or antibonding interaction is observed at the LUMO (−4.03 eV) position. However, if we look above LUMO (at about −3.65 to −3.05 eV), strong bonding interaction of *s* with *p* orbital and moderate antibonding interaction of *s* with *d* orbital are observed.

The COOP of Pt_4 presented in Fig. 8c shows that bonding interactions of *s* with *p*, *s* with *d*, and *p* with *d* orbitals are observed from −6.30 to −5.80 eV, which includes the HOMO (−5.88 eV) level. At the LUMO position (−3.92 eV), we found strong bonding interactions due to overlap of *s* and *p* orbitals. Antibonding interactions are also observed at LUMO position whose primary contribution is coming from the overlap of *s* with *d* orbital and a small contribution from the overlap of *p* with *d* orbital. Above the LUMO region, strong bonding interactions have been seen due to overlapping of *s* orbital with *p* orbital in the energy range −2.60 to −2.00 eV. Antibonding states, though feeble compared to its bonding counterpart, are formed in the same region due to overlapping of *s* with *d* orbital and *p* with *d* orbital in the energy range −4.10 to −3.55 eV. The COOP diagrams for n=5–10 are included in the supplementary information (Fig. S6 of supplementary data). For clusters n>4, the most significant contribution of antibonding state is originated due to the *p* and *d* orbital overlapping followed by *s* and *d* orbital overlapping. However in the case of bonding state, *s* and *p* orbital overlapping plays the fundamental role. It should be noted here that neither bonding nor antibonding states are formed in the LUMO position of Pt_6, Pt_7, and Pt_9.

Conclusions

In summary, we have studied the structure, stability, reactivity, and optical properties of small platinum clusters, Pt_n (n=2 to 10). With cluster size, the binding energy per atom of the cluster increases. Our calculated electron affinity values and vibrational frequencies are in agreement with the available experimental results. Electron affinity and electrophilicity show similar variation with cluster size. Our calculated electrophilicity values suggest that Pt_7 cluster is more stable, i.e., less reactive than its neighboring clusters. The highest peak of the Raman spectra is shifted toward the low frequency region with increasing size of the cluster. By paying attention to the molar absorption coefficient, we see that the overall evolutionary trend of the most prominent peak occurs at high wavelength (or low energy) side once we move toward larger cluster size. The total DOS up to HOMO position is primarily contributed by *d* orbital with a small contribution from *s* orbital, however in the above LUMO region the main

contribution is coming from *s* orbital along with *p* orbital which was missing in the former case. Our COOP analysis suggest that below LUMO level the bonding states are formed due to the overlapping of *s* orbital with *p* orbital and sometimes augmented by the overlapping of *p* with *d*, however, above the LUMO level it is due to the overlapping of *s* orbital with *p* orbital. Except for small clusters, major contribution for the antibonding states is coming from the overlapping of *p* and *d* orbitals, and minor contribution is from either the overlapping of *s* and *d* orbitals (below LUMO level) or from the overlapping of both *s* with *p* and *s* with *d* (above LUMO level) orbitals.

Acknowledgments Dr U. Sarkar acknowledges the support from SHARCNET Canada for providing the computational facilities for this research work.

References

1. Sarkar U, Blundell S (2009) Structure and thermodynamics of Fe_{55}, Co_{55}, and Ni_{55} clusters supported on a surface. Phys Rev B 79: 125441–7
2. Eberhardt W (2002) Clusters as new materials. Surf Sci 500:242–270
3. Vajda S, Pellin MJ, Greeley JP, Marshall CL, Curtiss LA, Ballentine GA, Elam JW, Mucherie SC, Redfern PC, Mehmood F, Zapol P (2009) Subnanometre platinum clusters as highly active and selective catalysts for the oxidative dehydrogenation of propane. Nat Mater 8: 213–216
4. Bell AT (2003) The impact of nanoscience on heterogeneous catalysis. Science 299:1688–1691
5. Bond GC (1991) Chemistry of the platinum group metals: recent developments. Elsevier, Amsterdam
6. Vielstich W, Lamm A, Gasteiger H (2003) Handbook of fuel cells: fundamentals, technology applications. Wiley West, Sussex
7. Yuan Q, Zhou Z, Zhuang J, Wang X (2010) Pd–Pt random alloy nanocubes with tunable compositions and their enhanced electrocatalytic activities. Chem Commun 46:1491–1493
8. Tian N, Zhou ZY, Sun SG, Ding Y, Wang ZL (2007) Synthesis of tetrahexahedral platinum nanocrystals with high-index facets and high electro-oxidation activity. Science 316:732–735
9. Zhang J, Sasaki K, Sutter E, Adzic RR (2007) Stabilization of platinum oxygen-reduction electrocatalysts using gold clusters. Science 315:220–222
10. Xu Y, Shelton WA, Schneider WF (2006) Effect of particle size on the oxidizability of platinum clusters. J Phys Chem A 110:5839–5846
11. Ghanty TK, Ghosh SK (1993) Correlation between hardness, polarizability, and size of atoms, molecules, and clusters. J Phys Chem 97: 4951–4953
12. Bedamani N, Sarkar U (2014) A density functional study of chemical, magnetic and thermodynamic properties of small palladium clusters. Mol Simul 40:1255–1264
13. Dai D, Balasubramanian K (1992) Potential energy surfaces for Pt_3 + H and Pd_3 + H interactions. J Phys Chem 96:3279–3282
14. Morse MD (1986) Clusters of transition-metal atoms. Chem Rev 86: 1049–1109
15. Duncan TM, Zilm KW, Hamilton DA, Root TW (1989) Adsorbed states of CO on dispersed metals: a high-resolution solid-state NMR study. J Phys Chem 93:2583–2590
16. Martin TP, Bergmann T, Golich G, Lange T (1991) Evidence for icosahedral shell structure in large magnesium clusters. Chem Phys Lett 176:343–347
17. Parr RG, Yang W (1989) Density functional theory of atoms and molecules. Oxford University Press, Oxford
18. Parr RG, Pearson RG (1983) Absolute hardness: companion parameter to absolute electronegativity. J Am Chem Soc 105:7512–7516
19. Parr RG, Lv S, Liu S (1999) Electrophilicity index. J Am Chem Soc 121:1922–1924
20. Chattaraj PK, Sarkar U, Roy DR (2006) Electrophilicity index. Chem Rev 106:2065–2091
21. Parthasarathi R, Padmanabhan J, Elango M, Chitra K, Subramanian V, Chattaraj PK (2006) pK_a Prediction using group philicity. J Phys Chem A 110:6540–6544
22. Chattaraj PK, Sengupta S (1996) Popular electronic structure principles in a dynamical context. J Phys Chem 100:16126–16130
23. Ghanty TK, Ghosh SK (1996) A Density functional approach to hardness, polarizability, and valency of molecules in chemical reactions. J Phys Chem 100:12295–12298
24. Chamorro E, Chattaraj PK, Fuentealba P (2003) Variation of the electrophilicity index along the reaction path. J Phys Chem A 107: 7068–7072
25. Parthasarathi R, Elango M, Subramanian V (2005) Variation of electrophilicity during molecular vibrations and internal rotations. Theor Chem Accounts 113:257–266
26. Pan S, Sola M, Chattaraj PK (2013) On the validity of the maximum hardness principle and the minimum electrophilicity principle during chemical reactions. J Phys Chem 117:1843–1852
27. Chandrakumar KRS, Ghanty TK, Ghosh SK (2005) Ab initio studies on the polarizability of lithium clusters: some unusual results. Int J Quantum Chem 105:166–173
28. Jaque P, Toro-Labbé A (2002) Characterization of copper clusters through the use of density functional theory reactivity descriptors. J Chem Phys 117:3208–3218
29. Ayers PW, Proft FD, Geerlings P (2007) Comparison of the utility of the shape function and electron density for predicting periodic properties: atomic ionization potentials. Phys Rev A 75:012508–8
30. Ayers PW, Parr RG (2000) Variational principles for describing chemical reactions: the Fukui function and chemical hardness revisited. J Am Chem Soc 122:2010–2018
31. Poater A, Duran M, Jaque P, Toro-Labbe A, Sola M (2006) Validity of the minimum polarizability principle in molecular vibrations and internal rotations: an ab initio SCF study. J Phys Chem B 110:6526–6536
32. Barbatti M, Aquino AJA, Lischka H (2010) The UV absorption of nucleobases: semi-classical ab initio simulations. Phys Chem Chem Phys 12:4959–4967
33. Soler JM, Artacho E, Gale JD, García A, Junquera J, Ordejón P, Sánchez-Portal D (2002) The SIESTA method for ab initio order-N materials simulation. J Phys Condens Matter 14:2745–2779
34. Frisch MJ, Trucks GW, Schlegel HB, Scuseria GE, Robb MA, Cheeseman JR, Scalmani G, Barone V, Mennucci B, Petersson GA, Nakatsuji H, Caricato M, Li X, Hratchian HP, Izmaylov AF, Bloino J, Zheng G, Sonnenberg JL, Hada M, Ehara M, Toyota K, Fukuda R, Hasegawa J, Ishida M, Nakajima T, Honda Y, Kitao O, Nakai H, Vreven T, Montgomery JA Jr, Peralta JE, Ogliaro F, Bearpark M, Heyd JJ, Brothers E, Kudin KN, Staroverov VN, Keith T, Kobayashi R, Normand J, Raghavachari K, Rendell A, Burant JC, Iyengar SS, Tomasi J, Cossi M, Rega N, Millam JM, Klene M, Knox JE, Cross JB, Bakken V, Adamo C, Jaramillo J, Gomperts R, Stratmann RE, Yazyev O, Austin AJ, Cammi R, Pomelli C, Ochterski JW, Martin RL, Morokuma K, Zakrzewski VG, Voth GA, Salvador P, Dannenberg JJ, Dapprich S, Daniels AD, Farkas O, Foresman JB, Ortiz JV, Cioslowski J, Fox DJ (2010) Gaussian 09, Revision C.01. Gaussian, Inc, Wallingford

35. Becke AD (1993) Density-functional thermochemistry. III. The role of exact exchange. J Chem Phys 98:5648–5652
36. Lee C, Yang W, Parr RG (1988) Development of the Colic-Salvetti correlation-energy formula into a functional of the electron density. Phys Rev B 37:785–789
37. Perdew JJ, Yang W (1992) Accurate and simple analytic representation of the electron-gas correlation energy. Phys Rev B 45:13244–13249
38. Hay PJ, Wadt WR (1985) Ab initio effective core potentials for molecular calculations. Potentials for the transition metal atoms Sc to Hg. J Chem Phys 82:270–283
39. Wadt WR, Hay PJ (1985) Ab initio effective core potentials for molecular calculations. Potentials for main group elements Na to Bi. J Chem Phys 82:284–298
40. Hay PJ, Wadt WR (1985) Ab initio effective core potentials for molecular calculations. Potentials for K to Au including the outermost core orbitals. J Chem Phys 82:299–310
41. Barbatti M, Granucci G, Persico M, Ruckenbauer M, Vazdar M, Eckert-Maksić M, Lischka H (2007) The on-the-fly surface-hopping program system NEWTON-X: application to ab initio simulation of the nonadiabatic photodynamics of benchmark. J Photochem Photobiol A 190:228–240
42. Barbatti M, Granucci G, Ruckenbauer M, Plasser F, Pittner J, Persico M, Lischka H (2013) NEWTON-X: a package for Newtonian dynamics close to the crossing seam, version 1.4, www.newtonx.org
43. Taylor S, Lemire GW, Hamrick YM, Fu Z, Morse MD (1988) Resonant two-photon ionization spectroscopy of jet-cooled Pt_2. J Chem Phys 89:5517–5523
44. Fortunelli A (1999) Density functional calculations on small platinum clusters: Pt_n^q (n=1–4, q=0,±1). J Mol Struct THEOCHEM 493: 233–240
45. Grushow A, Ervin KM (1997) Ligand and metal binding energies in platinum carbonyl cluster anions: collision-induced dissociation of Pt_m − and $Pt_m(CO)_n$−. J Chem Phys 106:9580–9593
46. Yang SH, Drabold DA, Adams JB, Ordejon P, Glassford K (1997) Density functional studies of small platinum clusters. J Phys Condens Matter 9:L39–L45
47. Kumar V, Kawazoe Y (2008) Evolution of atomic and electronic structure of Pt clusters: planar, layered, pyramidal, cage cubic, and octahedral growth. Phys Rev B 77:205418–10
48. Tian WQ, Ge M, Sahu BR, Wang D, Yamada T, Mashiko S (2004) Geometrical and electronic structure of the Pt_7 cluster: a density functional study. J Phys Chem A 108:3806–3812
49. Gibson ND, Davies BJ, Larson DJ (1993) The electron affinity of platinum. J Chem Phys 98:5104–5105
50. Ho J, Polak ML, Ervin KM, Lineberger WC (1993) Photoelectron spectroscopy of nickel group dimers: Ni^-_2, Pd^-_2, and Pt^-_2. J Chem Phys 99:8542–8551
51. Ervin KM, Ho J, Lineberger WC (1988) Electronic and vibrational structure of transition metal trimers: photoelectron spectra of Ni^-_3, Pd^-_3, and Pt^-_3. J Chem Phys 89:4514–4521
52. Pontius N, Bechthold PS, Neeb M, Eberhardt W (2000) Femtosecond multi-photon photoemission of small transition metal cluster anions. J Electron Spectrosc Relat Phenom 106: 107–116
53. Wong K, Vongehr S, Kresin VV (2003) Work functions, ionization potentials, and in between: scaling relations based on the image-charge model. Phys Rev B 67:035406–9
54. Derry GN, Ji-Zhong Z (1989) Work function of Pt(111). Phys Rev B 39:1940–1941
55. Miller TM (2002) CRC handbook of chemistry and physics. CRC, New York
56. Mohajeri A, Alipour M (2011) On the optical, electronic, and structural properties of zinc sulfide nanoclusters. Int J Quantum Chem 111:3841–3850
57. Jansson K, Scullman R (1976) Optical absorption spectra of PtO and Pt_2 in rare-gas matrices. J Mol Spectrosc 61:299–312
58. Solov'yov IA, Solov'yov AV, Greiner W (2004) Optical response of small magnesium clusters. J Phys B Atomic Mol Opt Phys 37:L137–L145
59. Hughbanks T, Hoffmann R (1983) Chains of trans-edge-sharing molybdenum octahedra: metal-metal bonding in extended systems. J Am Chem Soc 105:3528–3537